The Planetary Science Journal, 2:223 (13pp), 2021 December https://doi.org/10.3847/PSJ/ac2250
© 2021. The Author(s). Published by the American Astronomical Society.
OPEN ACCESS

Taurid Stream #628: A Reservoir of Large Cometary Impactors

Hadrien A. R. Devillepoix[1], Peter Jenniskens[2,3], Philip A. Bland[1], Eleanor K. Sansom[1], Martin C. Towner[1], Patrick Shober[1], Martin Cupák[1], Robert M. Howie[1], Benjamin A. D. Hartig[1], Seamus Anderson[1], Trent Jansen-Sturgeon[1], and Jim Albers[2]
[1] School of Earth and Planetary Sciences, Curtin University, Perth WA 6845, Australia
[2] SETI Institute, 189 Bernardo Avenue, Mountain View, CA 94043, USA
[3] NASA Ames Research Center, Mail Stop 241-11, Moffett Field, CA 94035, USA
Received 2021 June 29; revised 2021 August 18; accepted 2021 August 18; published 2021 November 3

Abstract

The Desert Fireball Network observed a significant outburst of fireballs belonging to the Southern Taurid Complex of meteor showers between 2015 October 27 and November 17. At the same time, the Cameras for Allsky Meteor Surveillance project detected a distinct population of smaller meteors belonging to the irregular IAU shower #628, the s-Taurids. While this returning outburst was predicted and observed in previous work, the reason for this stream is not yet understood. 2015 was the first year that the stream was precisely observed, providing an opportunity to better understand its nature. We analyze the orbital elements of stream members and establish a size–frequency distribution from millimeter to meter size range. The stream is highly stratified with a large change of entry speed along Earth's orbit. We confirm that the meteoroids have orbital periods near the 7:2 mean motion resonance with Jupiter. The mass distribution of this population is dominated by larger meteoroids, unlike that for the regular Southern Taurid shower. The distribution index is consistent with a gentle collisional fragmentation of weak material. A population of meter-sized objects is identified from satellite observations at a rate consistent with a continuation of the size–frequency distribution established at centimeter size. The observed change of longitude of perihelion among the s-Taurids points to recent (a few centuries ago) activity from fragmentation involving surviving asteroid 2015 TX24. This supports a model for the Taurid Complex showers that involves an ongoing fragmentation cascade of comet 2P/Encke siblings following a breakup some 20,000 yr ago.

Unified Astronomy Thesaurus concepts: Meteor streams (1035); Fireballs (538); Short period comets (1452)

Supporting material: machine-readable table

1. Introduction

The Southern and Northern Taurid showers are part of a Taurid Complex of meteor showers with daytime and nighttime components, the nighttime showers of which spread from September to December along Earth's path (Jenniskens 2006; Brown et al. 2013). Whipple (1940) first identified comet 2P/Encke as the likely parent body. The comet now has evolved to a phase in the rotation of the nodal line that keeps its nodes far from Earth. However, this Jupiter-family comet moves in a short 3.3 yr orbit that is decoupled from Jupiter, which makes both the comet and meteoroid orbits relatively stable for long periods of time. The wide dispersion of the showers' longitude of perihelion requires a formation age at least 20,000 yr ago, the minimum time it takes to disperse the longitude of perihelion of the orbits as wide as observed.

Clube & Napier (1984) first suggested that the a large number of potential other parent-body asteroids were part of a Taurid Complex that originated from a giant comet breakup 20,000 yr ago. However, Jenniskens (2006) pointed out that these early proposed parent bodies appeared to be S- or O-class stony asteroids, instead, which evolved into Encke-like orbits from a source in the asteroid belt via the ν_6 resonance. The same conclusion was also reached more recently by Popescu et al. (2014) and Tubiana et al. (2015).

Original content from this work may be used under the terms of the Creative Commons Attribution 4.0 licence. Any further distribution of this work must maintain attribution to the author(s) and the title of the work, journal citation and DOI.

Jenniskens (2006) and Jenniskens et al. (2016c) also noticed that there was no mirror image between Taurid shower component nodes in northern and southern branches, suggesting that meteoroids did not survive long enough to fully disperse their nodes around the original orbit. A full precession of the nodal line takes about 5000 yr; hence, individual shower components in the South and North branches are likely younger than 5000 yr. Instead, Jenniskens (2006) proposed that a more restrictive set of possible parent bodies with semimajor axis close to the 2.22 au of comet 2P/Encke was responsible and the 20,000 yr old stream now reflects the current dispersion of these smaller parent bodies that continue to generate Taurid meteoroids in the recent past. One possible parent was identified as asteroid 2004 TG10, now known to be a 1.3 km large object ($H = 19.4$) with low 0.018 albedo.

This idea that the Taurid complex is active as a whole, and is not just the remnant of a single 20,000+ yr old breakup, is supported by the orbital analysis done by Whipple & El-Din Hamid (1952). Long before modern orbital integrators and the introduction of orbital similarity criteria D (Southworth & Hawkins 1963; Drummond 1981), they were able to identify a group of Southern Taurids that dynamically converged 1400 yr in the past. To explain why Encke did not match the orbit of the group, they suggested that the stream of material could have come from a companion, which could have itself separated from Encke earlier. More recently, Olech (2016) reported two large bolides entering the skies of Poland on 2015 October 31. The meteoroids have very similar orbits ($D_D = 0.011$), and the authors identify two asteroids (2005 UR and 2005 TF50) as potential members of the stream. Using a backward integration,

Table 1
Predicted Returns of the Taurid Swarm

Year	Δ_M	Observations
1995	+29°	Spurný (1997)
1998	−13°	Beech et al. (2004)
2005	+11°	Dubietis & Arlt (2007); Shrbený & Spurný (2012); Olech et al. (2077)
2008	−30°	SonotaCo. (2009)
2012	+35°	Madiedo et al. (2014)
2015	−07°	This work; Spurný et al. (2017); Olech et al. (2077)
2022	+17°	Upcoming return

Note. Updates for recent years are published at the website https://www.cantab.net/users/davidasher/taurid/swarmyears.html, accessed 2017 May 16.

they show that these four objects (two meteoroids and two near-Earth objects) have their orbital elements converge 1500 yr ago, in good agreement with Whipple & El-Din Hamid (1952). That does not exclude that the bolides originated from one of the two asteroids in more recent times.

The 2015 bolides were part of an outburst of fireballs that is a repeating phenomenon for the Southern Taurid complex in late October and early November. Every 3+ yr, there is a significant uptick of Taurid fireballs (Table 1). There is no clear link to the times when comet Encke returns to perihelion. Instead, it appears that a cloud of meteoroids remains concentrated around a certain position (range of mean anomaly) along the orbit. Olech et al. (2077) reported on Taurids observed in the Polish Fireball Network in 2005 and 2015 and found that over 100 fireballs moved in similar orbits to asteroid 2015 TX24. Similarly, Spurný et al. (2017) found that 113 out of 144 Taurid fireballs observed by the European Network (EN) in 2015 had similar orbital elements and suggested that both asteroids 2015 TX24 and 2005 UR were associated with this stream, and possibly 2005 TF50, arguing that these several-hundred-meter-diameter bodies represented an extension of the population of bodies seen among the observed fireballs.

Froeschle & Scholl (1986) first suggested that meteoroids can be trapped by strong mean motion resonances (MMRs) with Jupiter. Material trapped in an MMR is prevented from undergoing full nodal precession, explaining concentrations of dust in mean anomaly over long periods of time. Asher et al. (1993) suggested that this occurred to some Taurids trapped in 7:2 MMR with Jupiter. The expected periodic signature of outbursts was later verified by Asher & Izumi (1998). Their model is successful at explaining enhanced activity in years when Earth comes within $\Delta_M \in \pm 30°/40°$ of the resonance center in mean anomaly (Table 1). Asher & Izumi (1998) also published future and past year outburst predictions by his model.

Jenniskens et al. (2016a) have identified this shower in 2010–2013 Cameras for Allsky Meteor Surveillance (CAMS) data as #628 in the IAU Working List of Meteor Showers, and they called it the s-Taurids (IAU code *STS*). We note that the "new stream" of Spurný et al. (2017) corresponds to the same IAU #628. Hereafter meteor shower IAU #2 (codenamed STA) refers to the "regular" Southern Taurids, IAU #628 (codenamed STS) designates the resonant Southern Taurid branch (s-Taurids), and the Southern Taurid Complex encompasses members from both substreams.

Spurný et al. (2017) outlined a correlation between size and strength: larger bodies among the 2015 Taurids tend to be more fragile. If so, that would imply that meter-sized objects would break at such high altitudes in Earth's atmosphere that they might be recognized in satellite observations. More recently, Borovička & Spurný (2020) found from a sample of 16 studied Taurid fireballs that the meteoroids >10 cm in size had low tensile strength, less than 0.01 MPa, and a density less than 1 g cm^{-3}. Smaller meteoroids contain a higher fraction of materials up to 0.3 MPa in strength.

With an eye on the upcoming 2022 return of the s-Taurids, we present in this paper observations of the enhanced 2015 Taurid fireball activity as observed by the Desert Fireball Network (DFN) in Australia and by the CAMS network in California. We investigate changes in the orbital elements along Earth's path, the stream's semimajor axis distribution, and the particle size distribution of the stream in order to better understand its relationship to comet 2P/Encke and other Taurid Complex parent bodies.

2. Data and Methods

DFN and CAMS survey meteoroid impacts at different sizes ranges: CAMS has the sensitivity to detect large numbers of small millimeter-tocentimeter-size grains, while the DFN takes advantage of a large collecting area to catch centimeter-to-decimeter-scale meteoroids, at the cost of lower sensitivity. When it comes to observing a bright meteor shower like the Taurids (Figure 1), the two systems complement each other well.

2.1. DFN

In 2015, the Australian DFN covered 1.5 million km^2 of sky viewing area, established around 30°S latitude (Howie et al. 2017a). Each DFN observatory comprises a high-resolution still imaging system: a 36 MP digital camera (Nikon D800, D800E, or D810), associated with a Samyang 8 mm f/3.5 fish-eye lens, taking 25 s exposures at 6400 ISO. In 2015 all observatories operated with these settings. The field of view of the cameras is all-sky, except for a crop of 10° on the horizons of long sides of the sensor (usually North and South). The pixel size is 119 s of arc in the center, decreasing toward the edges (87 s of arc at 5° elevation). The cameras are sensitive to stellar magnitude 0.5 for meteors (7.5 for stars) and reliably detect meteors that are brighter than apparent magnitude −1.5 for >0.9 s.

Meteor events are automatically detected in the images by the software procedures described by Towner et al. (2020). Astrometric measurements are performed in the same manner as described by Devillepoix et al. (2018), resulting in measurements precise down to 1–2 minutes of arc. The triangulation of meteor trajectories is performed using a weighted straight line least-squares approach, similar to the one described in Borovička (1990). In order to get an appropriate entry velocity for the meteoroid, an extended Kalman smoother is applied to the positional data, throughout the visible bright flight (Sansom et al. 2015). This method also yields statistical uncertainties that encompass both model errors and measurement errors. These results are crucial for initializing orbit determination, as orbital parameters, like the semimajor axis and eccentricity, are very sensitive to the errors in initial velocity. The heliocentric orbits of the meteoroids are determined using a backward integration from the start of the visible bright flight. The meteoroid is back-tracked through the upper layers of the atmosphere and out of the sphere of influence of Earth to a distance of one Hill sphere (Jansen-Sturgeon et al. 2019). Uncertainties on the orbital parameters are computed using a Monte Carlo method based on the uncertainties of the first velocity vector observed.

The DFN data reduction pipeline uses aperture photometry on the fireball track to calculate brightness. Doing photometry on the reference stars used for astrometry yields the instrumental zero-point of each camera, accounting for extinction and vignetting. The fireball brightness is converted into magnitudes by accounting for the different exposure times: the effective exposure time for stars is typically 11.2 s (25 s exposure modulated by the liquid crystal shutter), and 0.06 s or 0.02 s for a fireball shutter break (see Howie et al. 2017b for details on the action of the liquid crystal shutter). Apparent magnitude is converted to absolute (for constant distance of 100 km) after triangulation, using the observation range. The main limitation on this technique is the saturation of the sensor, which typically happens when the fireball exceeds apparent magnitude −6. Blooming of the trail enables brightness measurements out to about −10 mag.

The main use of photometric measurement in the present study is to calculate meteoroid strength and to get a zero-order mass estimate. As detailed by Brown et al. (2016), the peak brightness instant of a fireball is a good indicator of catastrophic fragmentation, and therefore a reasonable proxy for calculating a bulk tensile strength for the entering body. This method is more robust to instrumental bias than the PE criterion introduced by Ceplecha & McCrosky (1976) and has the advantage of being inferred directly from observable parameters (no mass calculation involved). We therefore use the following relation from Bronshten (1981) to calculate tensile strength S: $S = \rho_{\rm atm} v^2$, where $\rho_{\rm atm}$ is the density of the atmosphere estimated using the *NRLMSISE-00* atmospheric model (Picone et al. 2002). Parameter v is the velocity at that instant calculated by the Kalman smoother described by Sansom et al. (2015). The main limitation of the method comes from the uncertainty on the instant of peak brightness, dominated by the sampling rate (10 Hz), which translates into 2 km of altitude for the average Taurid, or a ≃1.3 factor in strength.

Thanks to the continental scale of the network, operational and weather biases are mitigated by the large collecting area and observation time. However, a consequence of this is that precisely determining the surveying area probed by the instrument is difficult. Calculating probing area as a function of time may be done accurately and relatively easily when a small number of narrow angle optics are used, such as described in Blaauw et al. (2016). But even at a basic level, this kind of work with all-sky cameras spaced on a continent-scale network is more tricky, and debiasing the DFN data set to get precise fluxes will be the subject of a future paper.

The DFN observatories, combined with the data reduction methods described above, have led already to multiple meteorite recoveries: Creston (Jenniskens et al. 2019), Murrili (Sansom et al. 2020), and Dingle Dell (Devillepoix et al. 2018), as well as three more recent (not yet published) recoveries. These successes in precisely pinpointing the location of meteorites are good indications that the data reduction process is free of major systematic issues.

2.2. CAMS

The main goal of CAMS is to map the presence of meteor showers of +4 to −5 mag meteors throughout the year. In 2015 November, CAMS networks had been established in California, Arizona, Florida, the BeNeLux, and New Zealand. Most CAMS networks are on the northern hemisphere, but they experienced a relatively small number of cloudy days that year. CAMS methods are described in detail in Jenniskens et al. (2011). In brief, CAMS utilizes a network of analog low-light video cameras, mostly Watec Wat902H2 Ultimate cameras with $30° \times 20°$ field of view each and +5.4 stellar limiting magnitude. Customized software detects the meteors, calibrates the background star field to obtain astrometric positions, and then combines such data from two or more stations to triangulate the meteor trajectory. CAMS yields more than 100,000 meteoroid orbits per year and has proven to be a very efficient tool for studying meteor showers and linking them to possible parent objects (Jenniskens et al. 2016a, 2016b, 2016c).

The high detection rate of meteors not assigned to showers by Jenniskens et al. (2016c), with geocentric entry speed <35 km s^{-1} from the antihelion source at the same time as the Taurid showers, provides a baseline of sporadic meteor shower activity that can be used to calculate the effective observing time due to weather. The CAMS flux data were debiasing by assuming a constant sporadic flux during the s-Taurid activity period. The main CAMS networks are situated at a latitude of $\phi = +37°$, where the Southern Taurid radiant is up almost all night in early November and the mean altitude of the Southern Taurid radiant is $hR \simeq 40°$. This results in a correction factor of $1/\sin(hR) = 1.35$ to get the equivalent zenithal hourly rate. For scaling the distribution we use the flux density of Grün et al. (1985), $f_G = 6.85 \times 10^{-8} > 1$ g meteoroids m^{-2} yr^{-1}, and the correction factor between interplanetary and top of the atmosphere $S = 0.67$ of Moorhead et al. (2019). From this, we can calculate the influx of s-Taurid on Earth as

$$N(\#628 > 1\ \text{g impacts on Earth}) = \frac{n}{m} * \frac{1}{\sin(hR)} * f_G * S * 2 * \Delta\lambda_\odot * \text{X}-\text{section}_{\rm Earth}.$$

In this formulation $\Delta\lambda_\odot$ is the exposure time to the shower as observed by CAMS, and the factor of 2 is there to compensate that a surface at the top of the atmosphere is effectively twice the collecting area of the model randomly tumbling plate of Moorhead et al. (2019). In relation to a meteoroid stream, Earth's exposure to the stream can be effectively represented as a cross-section area defined by its radius.

The reported flux values are limited to a 1 g threshold mass using the observed magnitude distribution. The count of all sporadic meteors with the 25–30 km s^{-1} entry speed of Taurids was assumed to be exponential in shape of this magnitude interval, from which a detection probability function was derived by fitting an exponential slope to the bright end of the magnitude distribution and then dividing observed counts by the fit-predicted count. The fraction of completeness for magnitudes −1 and up was $P(m) = 1.00,\ 0.80 \pm 0.02,\ 0.37 \pm 0.01,\ 0.093 \pm 0.003,\ 0.014 \pm 0.002,\ 0.001\,1 \pm 0.0002$, and ∼5e−6. This probability function was then applied to the detected count of shower meteors to derive the magnitude size distribution of different Taurid Complex component showers.

3. Results

The 73 measured DFN orbits from the Southern Taurid Complex in 2015 are provided as an Appendix to this paper. The CAMS-derived Southern Taurid Complex orbits were released as part of the 2013–2016 CAMS data release and can be accessed via the project website (https://www.seti.org/cams) and via the Meteor Data Center. In 2015, CAMS detected $N = 10{,}942$ Southern Taurids ($N = 177 > 1$ g) in the range $\lambda_\odot \in [213.19,\ 234.25]°$. In the same period, 131,230 (Nspo $= 1193 > 1$ g) sporadic meteors were recorded.

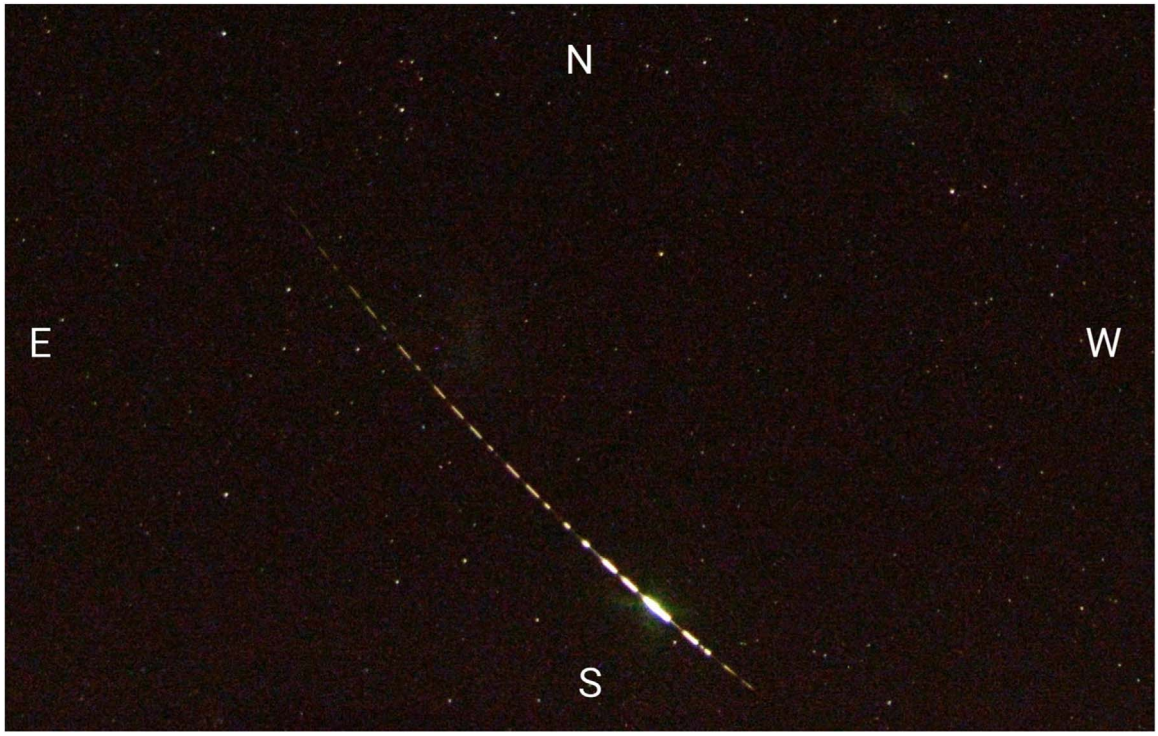

Figure 1. DN151104_01: a 2.6 s s-Taurid observed at Hughes siding in the Nullarbor plain, near the Magellanic Clouds. This is a crop of the original all-sky picture. The meteoroid experiences a catastrophic fragmentation at 74 km altitude, shortly before the meteor faded.

3.1. Comparison of s-Taurids with Regular Southern and Northern Taurids

The s-Taurid shower stands out well from other Southern Taurid complex meteors by their geocentric speed. Figure 2 plots the geocentric speed and time (solar longitude) of all meteors associated with the Southern Taurid complex in both the CAMS (top) and DFN (bottom) data sets. Vertical white bands are due to cloudy weather with less-than-complete coverage. The data are split into two groups: the outburst years of 2012 and 2015 (Table 2), and the no-outburst years of 2010, 2011, 2013, 2014, and 2016. The 2012 encounter with the s-Taurids is $\Delta_M = 35°$ from the center of the resonance according to the model of Table 1. Hence, the weak detection of the s-Taurids in 2012 by CAMS implies an extension of this component until at least mean anomaly 35°, in agreement.

The outburst years show a component that produces a narrow range of geocentric entry speed at any given solar longitude, with a strong change in the speed as a function of time. This component is only weakly present in nonoutburst years (Figure 2). This component was earlier identified as shower #628, the s-Taurids (IAU code STS). The period of activity for this component is $\lambda_\odot \in [213, 234]°$.

The presence of this STS component is also evident in the 2015 DFN data (Figure 2), despite a lower number of orbits, as the STS stream largely dominates the Southern Taurid activity at fireball sizes. The change in velocity with solar longitude translates into a strong increase of perihelion distance with increasing solar longitude and a decreasing eccentricity. The semimajor axis and inclination of the orbits remain nearly constant, as does the longitude of perihelion.

Figure 3 shows the debiased STS rates for CAMS, along with that of the remaining STA and NTA streams. The rates are normalized to that of all sporadic meteors with speeds $<35\,\mathrm{km\,s^{-1}}$. This ensures that the total sporadic count reflects the observing conditions during that part of the night when the antihelion source is best observed. The sporadic apex and toroidal sources have been removed from the count. The 2015 STS count was compared to the sporadic meteor rate in 2015 only. The multiyear debiased distribution produced better-defined shower activity profiles than early results in Jenniskens et al. (2016b). The shower components identified in Jenniskens et al. (2016c) are still present. The STA and NTA shower profiles are different, an indication that the nodal line of individual meteoroid orbits did not fully rotate, as earlier pointed out.

3.2. Size–Frequency Distribution of the #628 STS Stream

Figure 4 shows the distribution of peak magnitudes in 0.5 mag intervals for CAMS-detected NTA, STA, and STS meteors. The STS population is significantly more skewed toward brighter meteors. The cumulative mass–frequency distribution as observed by CAMS (Figure 8) can be expressed as $N(>m) = am^{-b}$ with $a = 1.42 \times 10^5$ and $b = 0.94$ when expressed in grams. This is representative of the total influx of s-Taurids during the 2015 encounter.

The annual Southern and Northern Taurids have differential magnitude indices of $\chi \simeq 3.0$ (Figure 3); this is close to the typical value for JFC material ($\chi = 3.29 \pm 0.09$, as determined by Jenniskens et al. 2016c). On the other hand, s-Taurids have a much shallower distribution with $\chi = \sim 2.0$ (assuming a sporadic $\chi = 3.4$). This gives a differential mass index for the observable stream of $s = 1.75$ ($s = 1 + 2.5 \log(\chi)$).

The observed size distribution confirms that the s-Taurids are relatively rich in large meteoroids. Indeed, a study by Soja et al. (2011) on radar meteors observed by the Canadian Meteor Orbit Radar in 2005 (typical observed mass of 10^{-7} kg, which roughly corresponds to optical magnitude +7) failed to identify

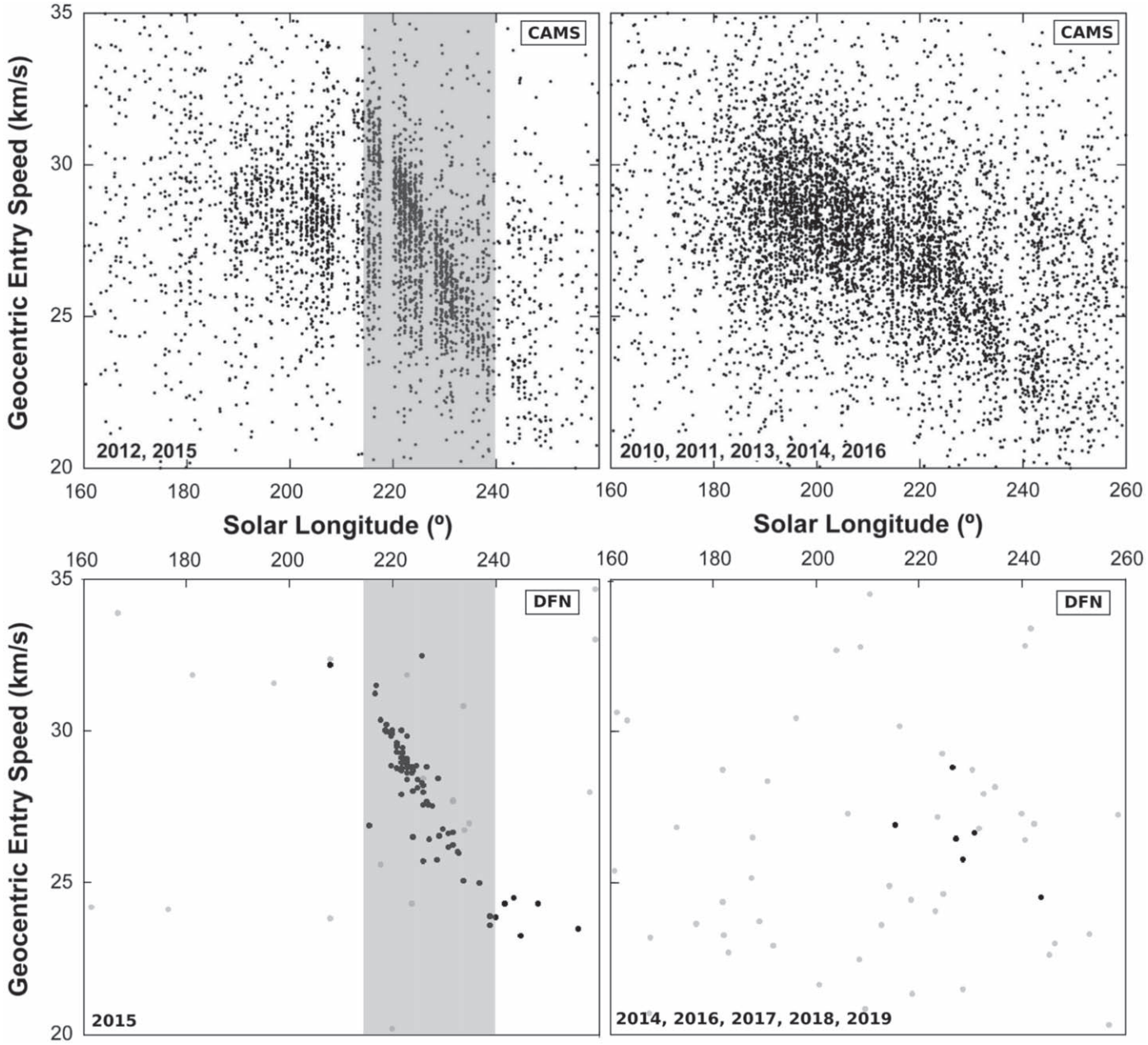

Figure 2. Detected meteors' geocentric entry speed as a function of solar longitude. STS activity years (left) are separated from other observation years (right). In DFN data, fireballs identified as Southern Taurids are marked in black against gray background fireballs. While the STS component of the Southern Taurids, recognized by its strong date–speed linear relationship, is visible in the meteor data (CAMS; top left), it is even more obvious at fireball sizes (DFN; bottom left).

the 7:2 resonance from regular Southern Taurids. They discuss that this is partly due to the poor constraints the radar observations put on the velocities (and therefore the semimajor axes), so it is not possible to distinguish STSs from STAs dynamically. Therefore, unless the STS outburst is strong enough to significantly skew the overall Southern Taurids rates, it is not detectable. Soja et al. (2011) do not provide an upper constraint on the STS/STA activity, but even without hard numbers this analysis confirms the trend shown in Figure 4: the STA branch dominates the STS branch at the low-mass end ($Mv_{\max} > -4$).

Beyond CAMS data, toward fireball sizes, flux density data for this stream become more scarce. The DFN and EN fireball networks do not yet have time–area debiasing information to calculate flux densities. The masses reported by Spurný et al. (2017) give an idea of the slope of the distribution at magnitudes below −9, where the EN sample appears to be complete (Figure 8). Although it is apparently shallower than the slope calculated by CAMS, the numbers are so small that the extrapolated flux agrees within 2 error bars (2σ). Even at these bright magnitudes there may still be an effect of the brightness-dependent variation in effective covering/reporting: the brighter the bolide, the further it can get detected and studied.

3.3. Strength of the Meteoroids in the #628 STS Stream

Figure 5 shows the altitude of peak brightness as a function of peak meteor magnitude. The result shows that larger meteoroids penetrate deeper into Earth's atmosphere before reaching peak brightness, as expected. Among CAMS-detected visual meteors,

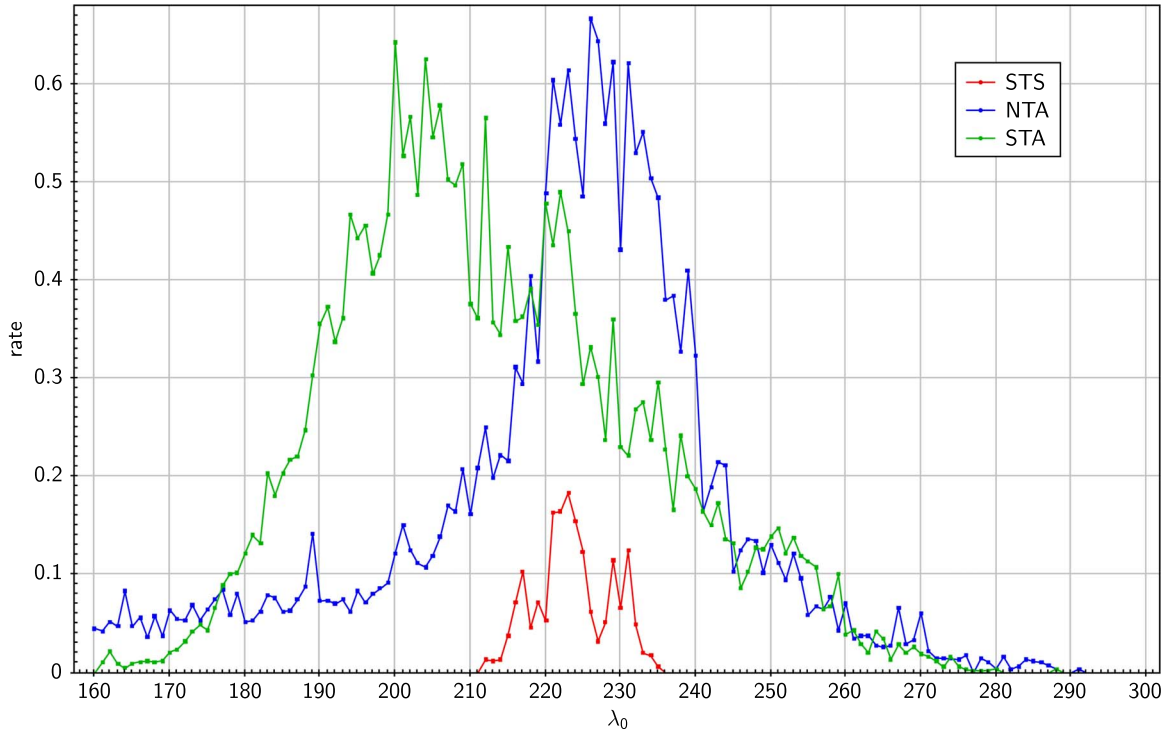

Figure 3. Debiased CAMS shower rates relative to that of sporadic meteors <35 km s^{-1} for shower 628 (STS), the Southern Taurids (STA), and the Northern Taurids (NTA), as a function of solar longitude.

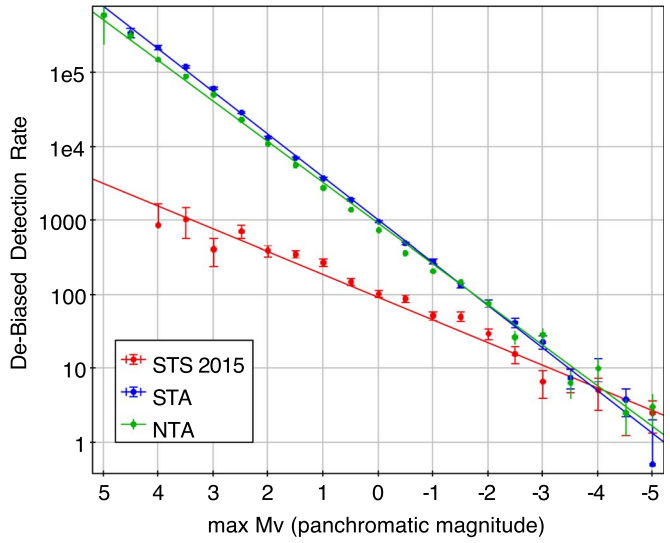

Figure 4. Peak magnitude frequency distribution for Southern Taurids substreams #2 STA, #17 NTA, and #628 STS. Resonant Taurids (STS branch) are generally larger than regular Southern Taurids (STA).

that is a fairly continuous trend. However, at the larger fireball sizes, meteoroid penetration enters a strength-dominated regime. The transition into the strength-dominated regime occurs at about −7 mag. In the strength-dominated regime, the altitude of peak brightness is independent of mass, although there is a weak trend that the largest meteoroids are weaker than the smaller meteoroids near this transition. All s-Taurids experience their peak brightness above 60 km altitude (Figure 5) and do not survive below 50 km altitude. The deepest penetrating fireball had a minimum height of 54.5 km, while the average end height of the DFN fireballs was 67.2 km (see Table A1). This is consistent with the results of Spurný et al. (2017).

3.4. Semimajor Axis of the Fireball Orbits

Figure 6 is an ecliptic orbit plot of all Southern Taurids observed by the DFN in 2015. The figure shows that most observed Taurid fireballs clustered in a tight stream with constant longitude of perihelion (all ellipses pointed in the same direction). These s-Taurids are shown in blue. This stream is highly stratified: they form a series of more or less concentric ellipses for fireballs detected at different solar longitude along Earth's orbit. Unlike most meteoroid streams, this stream appears to be narrower at aphelion than at perihelion. The dispersion of perihelion distances (q) of the blue orbits is 8.9% (one standard deviation), while the aphelion distance (Q) is dispersed by only 2.4%, and the semimajor axis (a) by 2.1%. a and Q are tightly correlated; a and q are not. The stream approaches the orbit of Jupiter near aphelion, suggesting that the secular perturbations responsible for the observed dispersion are strongest near aphelion, not near perihelion.

Figure 7 plots the semimajor axis of the 2015 Taurid fireballs measured in the DFN network as a function of solar longitude (time in the year). The DFN-derived orbits during solar longitudes 217.5 and 227.5 show a clear concentration of semimajor axis values around the mean semimajor axis $a = 2.234 \pm 0.007$ au with a standard dispersion of 0.041 au. The mean calculated error in the semimajor axis values is 0.034 ± 0.014 au, in good agreement with the observed dispersion if all these orbits have exactly the same semimajor axis of $a = 2.2563$ au corresponding to the 7:2 MMR with Jupiter (dashed line). This result confirms earlier conclusions from EN fireball observations reported by Spurný et al. (2017) that the meteoroids appear to be trapped in this resonance, and it demonstrates the accuracy of the semimajor axis calculations.

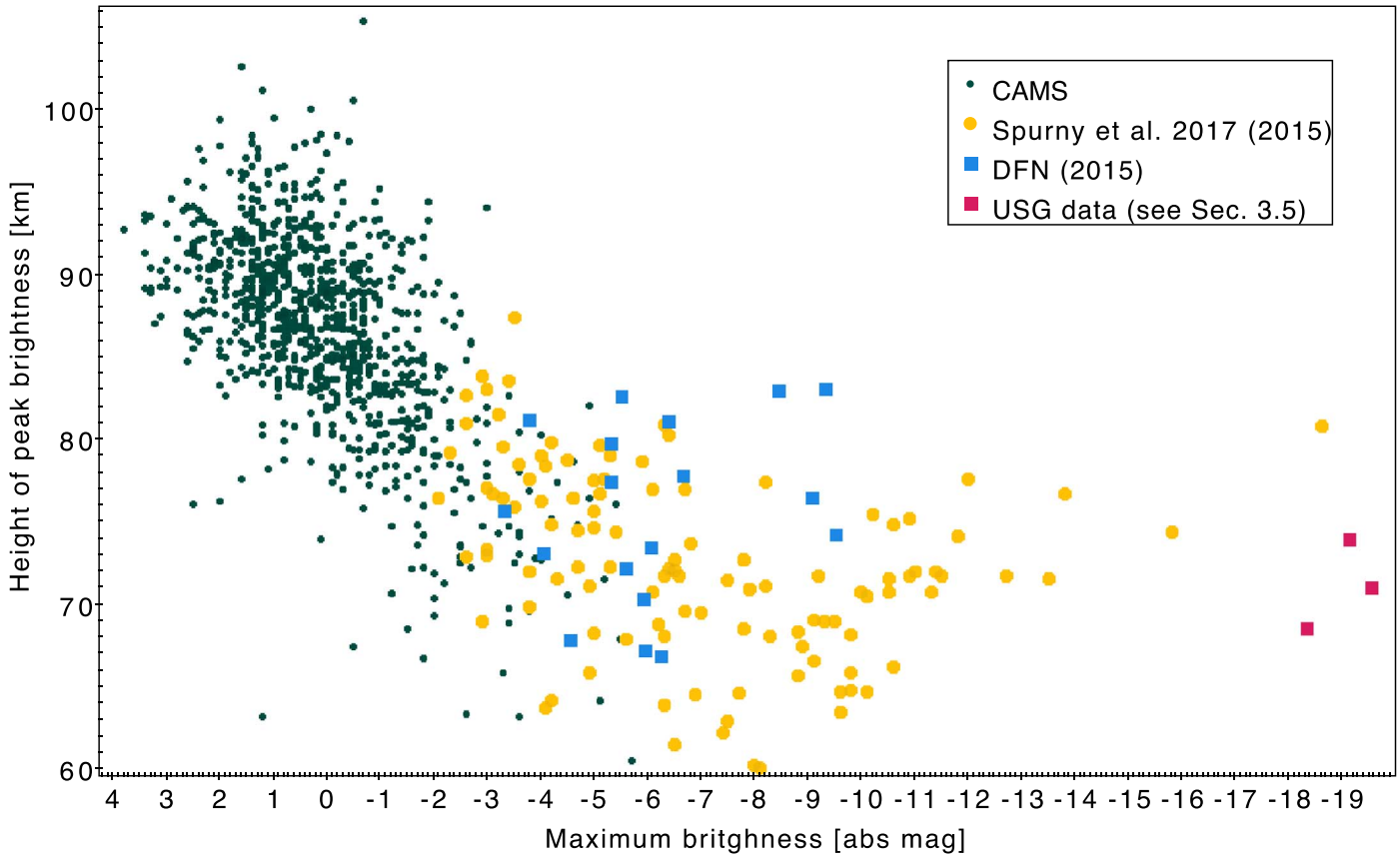

Figure 5. s-Taurids height of peak brightness as a function of brightness. DFN magnitudes may be slightly underestimated because of saturation issues.

Most of the observed dispersion in semimajor axis is due to measurement error. However, there is a small systematic error of -0.022 ± 0.007 au.

The fireballs shown in pink are outside the main dispersion. Most have slightly smaller semimajor axis, while three orbits just reach the orbit of Jupiter. A total of 52 of the observed trajectories have a semimajor axis within 2σ from the resonant value; 21 do not. Surprisingly, the latter scatter around the time of the outburst over 216.°5–231.°7 solar longitude (CAMS has 212°–235° range; see below), while the ones that are within 2σ from the resonant value scatter over the whole observing interval of 207.7–255.9 solar longitude. Hence, whether or not the trajectories scatter around the resonant value is not a mark of the s-Taurids; it is a mark of the Southern Taurids as a whole.

Some of the pink orbits may represent measurement errors in the initial velocity determination, or they are a more perturbed population of meteoroids that possibly already experienced some changes in semimajor axis due to encounters with the terrestrial planets. If so, they are likely part of the background Southern Taurids.

3.5. The Meter-size Population

Spurný et al. (2017) first pointed out that the stream contains meter-sized asteroids. Here, we will attempt to quantify this. The US government (USG) satellite sensors detect meter-scale impactors in Earth's atmosphere over the entire planet as a collecting area, or if a meteoroid stream is involved approaching from a given direction, that collection area is the projected Earth surface to that stream. These data are reported online on the NASA JPL fireball website.[4] Even with this large of a collection area, the chance of detecting impacts is small. Figure 8 shows the cumulative mass–frequency distribution from CAMS and DFN data. The USG-detected bolides are about −18 mag and brighter (Tagliaferri 1994). That leaves a large gap without debiased data.

Extrapolating the mass–frequency distribution established in Section 3.2, we predict 0.37 meteoroids > 940 kg impacting Earth during the 2015 s-Taurid episode. Indeed, the USG satellites detected no unusual number of fireballs in late October and early 2015 November. One bolide was detected on 2015 October 31, one on 2015 November 2, and one on 2015 November 13. No velocity components are reported, so we do not know the radiant or speed of these bolides.

However, there are data from multiple years of observation now. If any Taurids are among these impactors, we expect their penetration depth to be relatively shallow based on the size dependence shown in Figure 5. The observed centimeter-to-decimeter-sized meteoroids by CAMS, DFN, and EN show no significant decrease in peak height as sizes get larger.

The USG data only include the altitude of peak brightness. We started by filtering the USG data set by height of maximum brightness >60 km as a first pass to identify weak cometary impacts, as STS observed by the DFN breakup >66 km (Figure 5). We note that the stated peak brightness altitude from the sensors is generally reliable to about ±4 km,

[4] https://cneos.jpl.nasa.gov/fireballs/, accessed 2017 May 16.

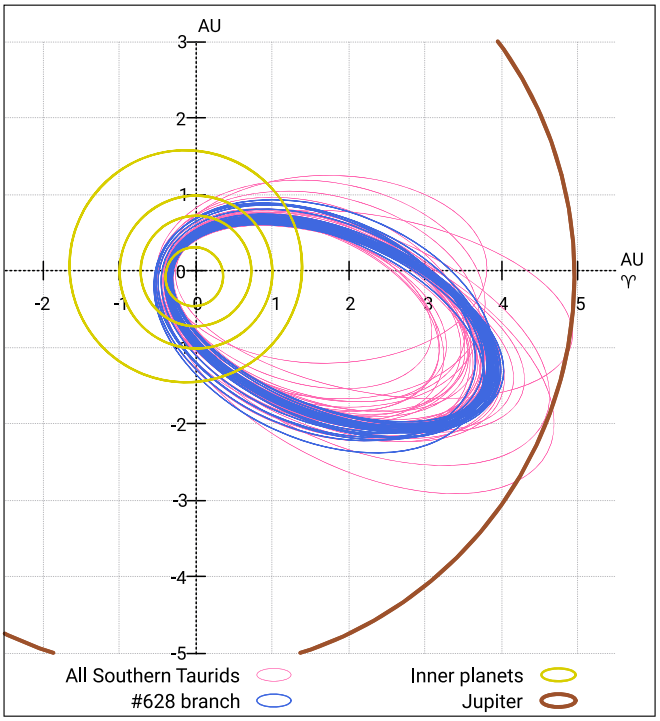

Figure 6. Ecliptic orbit plot of all Southern Taurids observed by the DFN in 2015 (pink) and the #628 branch (blue).

as shown by Brown et al. (2016), and that these altitudes are reported for most events from the beginning of 2005 onward. Detections are made at night, but also in daytime. As mentioned by Devillepoix et al. (2019), the typical energy report limit is 0.1 kT TNT; therefore, we exclude event *2011 August 4 07:25:57* (0.098 kT reported yield) from our analysis for detection significance issues. We are left with 10 significant events that fit the height criterion (Table 3). However, there are no velocity vectors reported for these events, so there is no direct dynamic link between any of these and the Taurid complex.

Nevertheless, 3 out of these 10 very weak meteoroids fall in the STS activity period, and even more remarkable, they happen in 2005 and 2015, two years during which strong STS activity has been reported, and are predicted by the model of Asher & Izumi (1998) (Table 1). In 2005, two events occurred in short succession. All three events suggest that the largest fragments in this stream are at solar longitude [213, 234]°. Given this, combined with data in Figure 3, these USG bolides occurred during the STS activity period. We confirm that these three events happened while the Southern Taurid radiant was above the local horizon.

Can these bolides signify a detection of the s-Taurids? Considering the very low number of events observed, we need to build a statistical test to assess the significance of this apparent rate increase during a swarm episode. Let us test the hypothesis H_1, "An airburst from weak material (main explosion >60 km) is more likely to happen during an STS activity period," against the null hypothesis H_0, "No increase in the rate of impacts from weak bodies can be observed during an STS activity episode." We define an STS swarm episode as a period that happens on a year predicted by the model of Asher & Izumi (1998), within the interval where the USG sensors have consistently observed airburst heights

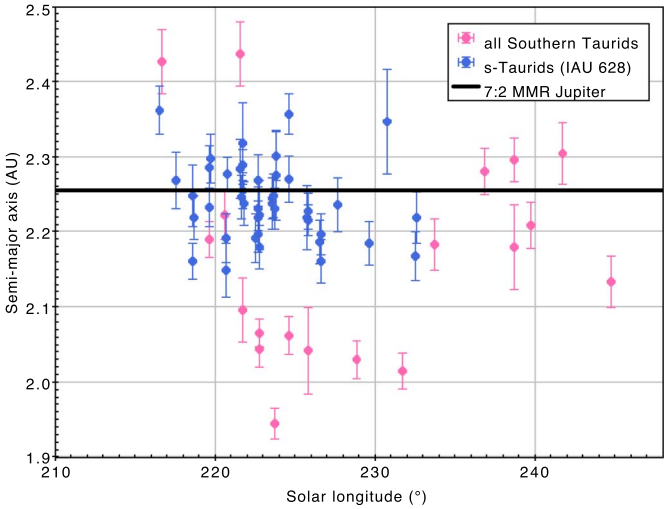

Figure 7. Semimajor axis measurements (with 1σ uncertainties error bars) of all Southern Taurid fireballs observed by the DFN 2015. Most are significantly higher than typical Southern Taurids, compatible with a 7:2 MMR with Jupiter (centered on 2.256 au).

(2005, 2008, 2012, 2015), and within the activity period observed by CAMS (solar longitude $\in$ [213, 234]°). We use the *rateratio.test R* package,[5] which implements the methods described in Fay (2010) to carry out the statistical test. At 95% confidence, the background weak meter-scale impact rate is [0.001, 0.005], compared to [0.007, 0.1] Earth$^{-1}\lambda_{\odot}^{-1}$ when $\lambda_{\odot} \in$ [213, 234]°, which corresponds to a weak impactor influx increase of [2.5, 55]× (see Table 4 for full test test data and results). The small p-value = 0.004 shows strong evidence against the null hypothesis (at 95% confidence).

Although we cannot definitely link any individual events with the Taurids, the apparent rate increase in meter-scale weak impactors during the STS outburst activity is statistically significant, and we can say that during an STS outburst episode Earth is more likely to get impacted by a meter-scale STS than a sporadic meteoroid of the same size. Over an s-Taurid episode, the number of >0.1 kT TNT of s-Taurid impactor is [0.15, 2.1] (Figure 8).

Adding this detection rate to the overall picture shows that the meteoroid size distribution does not change down to meter-size scale (Figure 8). This result implies that the #628 STS stream contains some of the largest meteoroids known to any cometary meteor shower.

Finally, it is possible that the USG satellite detections do not represent all large bolides in Earth's atmosphere. The European Network detected one superbolide during the 2015 outburst called `EN311015_180520` (Spurný et al. 2017). The observation of this 1300 kg bolide over a superbolide coverage area of roughly 0.1% Earth is statistically unlikely but not impossible (Figure 8). The `EN311015_180520` superbolide (0.17 kT TNT total kinetic energy) should have been well within the detection range of the USG sensors, but this bolide was not reported. A single mismatch is not indicative of a particular issue, as the USG sensors are known to have had as low as 70%–80% Earth coverage in the past (Brown et al. 2002). The USG sensors' s-Taurid flux could have been underestimated by a factor of 2 considering that both 2008 and 2012 were taken into account for the USG clear-sky

[5] https://cran.r-project.org/package=rateratio.test

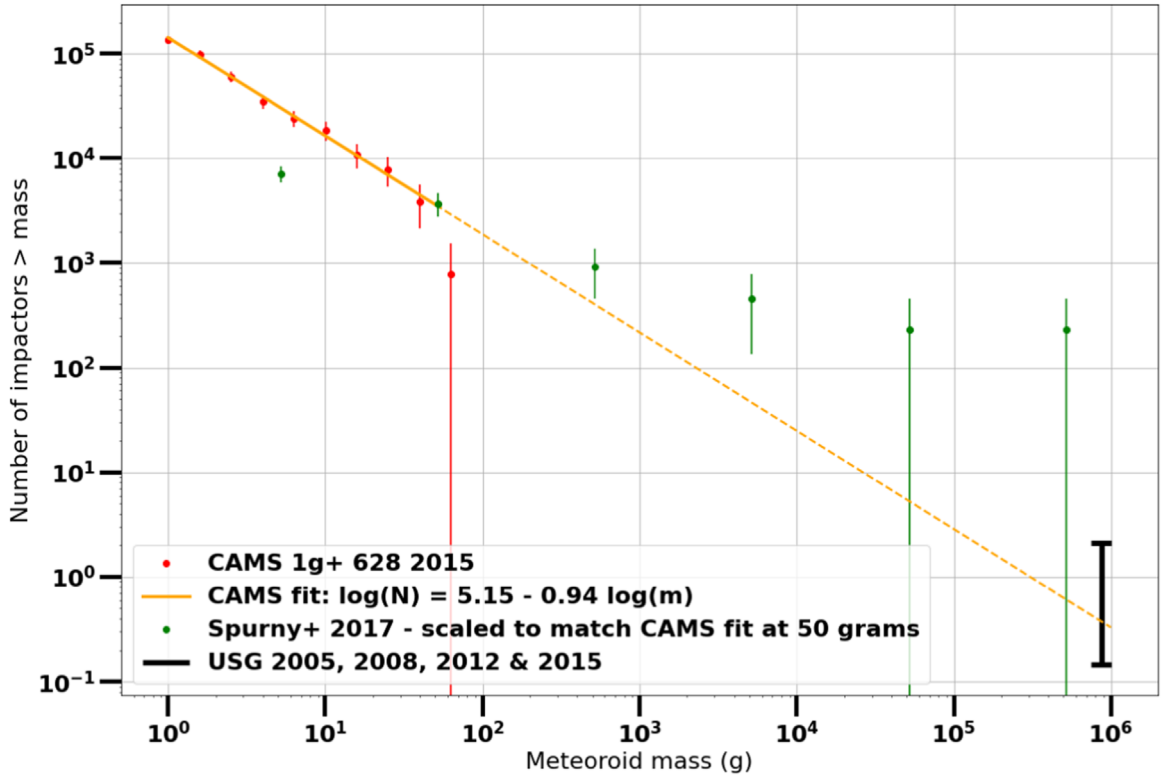

Figure 8. Cumulative mass–frequency distribution. CAMS > 1 g meteors left is fitted based on the 2015 data (see Section 3.2). The s-Taurid 2015 data of Spurný et al. (2017) are presented in green, with the event frequency scaled to match CAMS' at 50 grams. Note that the different slope for these data may not be real and could come from a brightness-dependent variation in effective covering area. The right-hand side estimate comes from three likely large s-Taurids observed by the USG sensors in 2005 and 2015.

Table 2
Proposed Parent Bodies for the s-Taurids

Object	Epoch (TDB)	a (au)	e	q (au)	i (deg)	Long. Ascen. Node (deg)	Arg. Peri. (deg)	Long. Peri. (deg)
2P/Encke	2015-08-04.0	2.215 2	0.848 3	0.336 0	11.781	334.568	186.547	161.115
2003 WP21	2020-12-17.0	2.262 0	0.784 9	0.486 6	4.295	37.654	124.030	161.390
2004 TG10	2020-12-17.0	2.233 4	0.862 0	0.308 3	4.183	205.073	317.381	162.454
2005 UR	2005-10-26.0	2.249 2	0.881 8	0.266 0	6.935	20.030	140.477	160.507
2005 TF50	2020-12-17.0	2.273 0	0.869 2	0.297 2	10.725	0.564	159.962	160.526
2015 TX24	2020-12-17.0	2.264 7	0.872 4	0.289 0	6.049	32.827	127.151	159.978
s-Taurids (DFN)	2015-11-05.1	2.237	0.847	0.358	5.45	42.72	115.70	158.31

calculations (Section 3.5), as these two years were quite distant from the resonance center. It could mean that the meter-scale s-Taurid is a factor of 2 larger than what we calculated here. That would still be consistent with a constant mass distribution index from centimeter to meter scale (Figure 8).

4. Discussion

4.1. Nature and Origin of the s-Taurids

The low magnitude distribution index ($\chi = 2.0$) and small differential mass index ($s = 1.75$) are atypical of most JFC showers. Such values point to a collisionally relaxed population, with equal combined cross-section area in each magnitude bin ($s = 1.67$), or a collisional cascade where each meteoroid is broken by a mass just big enough to do so ($s = 1.83$). This points to a very gentle collision process such as would be experienced during a cometary breakup of relatively strong material with intrinsic low-s size distribution. High-velocity collisions in the interstellar medium or other aging processes like grain charging and thermal cycling did not significantly affect the size distribution index of this population of meteoroids. That means that the stream is relatively young and was born from relatively strong cometary material. Weak cometary material breaks into very steep distributions toward small particles (Jenniskens 2006).

The unusually large number of shower fireballs detected by DFN and EN points to the presence of large meteoroids in this stream. Continuation of the particle size distribution to larger sizes implies a population of meter-sized objects in this stream that appears to have been detected in USG satellite observations. The presence of such large bodies in the stream is consistent with the material being relatively strong for cometary material in general. This stream is currently a major contributor to the overall population of large weak meteoroids. If the USG statistics are

Table 3
14 High-altitude (>60 km) Meteoroid Airbursts Observed by the USGS

Peak Brightness Time ISO UTC	$\lambda_\odot$ (deg)	Latitude (deg) (N+)	Longitude (deg) (E+)	Altitude (km)	Total Impact Energy (kilotons TNT)	Size (m)
2015-10-31 11:34:30	**217.51**	**9.0**	**−138.0**	**71.0**	**0.29**	**1.5**
2015-06-10 17:43:03	79.32	−11.5	−161.9	61.1	1.0	
2013-08-12 18:08:02	140.00	−34.4	118.2	66.6	0.15	
2012-02-12 05:25:52	322.72	−31.7	54.9	61.0	0.41	
2011-01-21 15:11:43	301.07	18.9	−44.6	61.0	0.23	
2010-12-09 02:54:07	256.76	−54.5	−169.7	66.0	0.2	
2005-12-24 15:30:26	272.85	−54.0	17.3	66.0	0.51	
2005-11-02 07:04:32	**219.89**	**33.9**	**−154.9**	**68.5**	**0.11**	**1.1**
2005-11-02 05:16:47	**219.81**	**22.9**	**−123.8**	**74.0**	**0.21**	**1.3**
2005-04-06 01:30:24	16.28	−42.7	154.6	70.0	0.1	
*2011-08-04 07:25:57	131.44	−40.7	−86.7	63.0	0.098	
2004-01-02 04:27:59	281.05	−28.2	3.2	63.0	0.39	
1999-06-25 06:27:41	**93.30**	**50.0**	**121.0**	**69.0**	**0.37**	
1999-01-02 18:25:51	281.93	47.0	103.0	65.0	0.12	

Note. No velocity information was provided for the events presented here. Bolded rows show events that fall within the STS activity period. The four events at the bottom are excluded for statistical significance reasons (see the text). Size is calculated from the energy, assuming that the velocity is equal to the mean STS velocity observed by the DFN at the same given solar longitude (see Table A1) and the 1600 kg m^{-3} bulk density estimated by Babadzhanov & Kokhirova (2009).

representative of larger cometary impact hazards, the s-Taurids dominate the flux when they are active, increasing the impact risk by $[2.5,\ 55] \times (2\sigma)$, and overall they represent a significant fraction of all large cometary impactors, even though their activity period is only a few weeks every couple of years!

Our measured DFN fireball mean semimajor axis of 2.234 ± 0.007 au is 0.019 au higher than the semimajor axis of 2P/Encke but 0.022 au lower than the $a = 2.2563$ au corresponding to the 7:2 MMR with Jupiter. It is also 0.031 au lower than the current semimajor axis of 2015 TX24. Natural oscillations of semimajor axis are about 0.03 au in this part of the asteroid belt (Nesvorný & Morbidelli 1998), so the motion of all objects will be affected by the MMR. If the breakup happened in the resonance with small relative ejection velocities, it is likely that the resonance prevented the dispersion of the dust by avoiding Jupiter's presence at aphelion when the dust was there.

Spurný et al. (2017) argued that the s-Taurids are the product of fragmentation event (of 2004 TG10?) at about 3.6 au distance from the Sun, where the fireball orbits have lowest dispersion, with relatively high ejection speeds of 1.5 km s^{-1}. The observed asteroids 2005 TF50, 2015 TX24, and 2005 UR (and 2004 TG10) were created in that event and now have evolved along the rotation of the nodal line, now located 2000, 2300, and 2400 yr in rotation behind 2004 TG10. Material not trapped in the 7:2 MMR has since been lost.

That high ejection speed of 1.5 km s^{-1} is contrary to the gentle breakup conditions implied by the particle size distribution we measured in this paper. It would also suggest that much of the material was ejected into orbits outside of the MMR and material would still be dispersing rather quickly along mean anomaly over time. Instead, we see that dust is confined in a narrow range of mean anomaly. The best handle on age comes from the work by Whipple & El-Din Hamid (1952) and Olech (2016), who found that individual fireball orbits originated from a common orbit about 1500 yr ago. However, if the MMR is involved, this age may be an upper limit only.

On closer inspection, we find that the change of argument of perihelion with node does not align all three bodies (Figure 9). As noticed before by Spurný et al. (2017), the longitude of perihelion is not quite constant in the s-Taurids stream. Instead, the trend of argument of perihelion points directly at asteroid 2015 TX24, which is only 3°.5 further in node than the range of DFN fireballs observed. A few EN fireballs cover the node of 2015 TX24. 2015 TX24 is also close in position to the nodal dependence seen with perihelion distance, eccentricity, and inclination, but those parameters can scatter more easily and that difference may merely reflect the change in orbital elements needed to intersect Earth's orbit.

Asteroids 2005 UR and 2005 TF50 have similar longitude of perihelion to 2015 TX24 but do not fall along the trend line seen among the meteoroids. We conclude that these larger asteroids are not simply fragments of this stream as proposed by Spurný et al. (2017).

A likely scenario is that we are seeing recent activity from a breakup involving surviving asteroid 2015 TX24. 2015 TX24 now has a semimajor axis of 2.2647 au (epoch 2020 December 17.0 TDB). That puts it within the normal semimajor axis oscillation of ±0.03 au from the resonance. Solar radiation pressure will slightly increase the semimajor axis of the DFN meteoroids, but if the ejection conditions were slightly lowering the semimajor axis, this could have been compensated. It is possible that the change of longitude of perihelion away from the node of 2015 TX24 is due to the influence of the 7:2 MMR. Presumably, the further the meteoroid node now is from 2015 TX24, the stronger the influence of the resonance. The precision of the semimajor axis is not good enough to verify that. If so, that could mean that the breakup happened rather recently, perhaps as recently as a few centuries ago.

This supports a model for the Taurid Complex showers that involves an ongoing fragmentation cascade of comet 2P/Encke siblings that were created following a breakup some 20,000 yr ago (Jenniskens 2006). In this scenario, 2015 TX24 broke with 2005 UR and 2005 TF50 from a larger precursor body about 1500 yr ago, and in the past few centuries a further breakup of 2015 TX24 created the fragments observed as the s-Taurids today. Asteroid 2003 WP21 does not belong to this group and was created earlier.

It is more difficult to understand how we could be seeing activity from comet 2P/Encke. In that case, the resonance must have more dramatically changed the nodal line. Comet

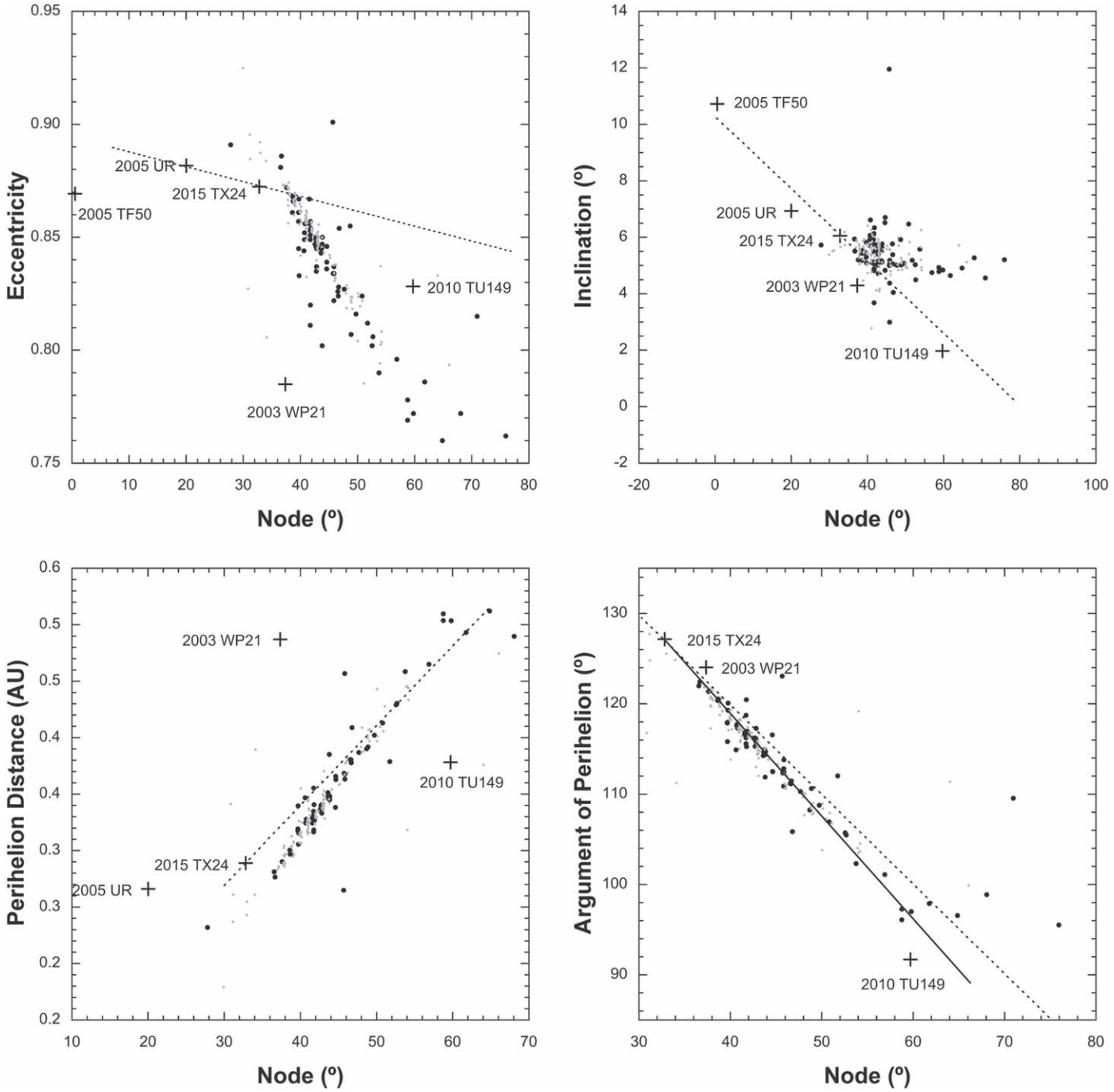

Figure 9. Orbital elements of #628 meteoroids observed by DFN (black circles) and EN (gray circles; Spurný et al. 2017), put in context with the discussed possible parent bodies for the stream (Table 2).

2P/Encke would be expected to cause meteoroid activity centered on $\lambda_{\odot} = 224\overset{\circ}{.}6$, using method "H" of Hasegawa (1990), implemented by Neslusan et al. (1998). However, Encke now has nodes close to perihelion near Mercury and aphelion in the asteroid belt. Comet Encke's orbit has changed its longitude of perihelion significantly over the past two centuries. In 1769, the node was at $157\overset{\circ}{.}46$, Pi $= 159\overset{\circ}{.}19$. In 2020, the node is at $154\overset{\circ}{.}55$, Pi $= 161\overset{\circ}{.}11$. That rate of change is about the same as seen in the meteor stream. Around AD 1700, the longitude of perihelion of Encke was the same as that of the core of the s-Taurids. If we are seeing meteoroids ejected from 2P/Encke in the century around AD 1700, there must have been a subsequent dramatic change of the nodal line.

It is not clear whether or not the periodic nature of the s-Taurids is due to the 7:2 MMR with Jupiter, other than preventing close encounters with Jupiter. The mean semimajor axis of the meteoroids appears to be related to that of its parent body. It is perhaps possible that the dust was released with very low relative ejection speeds and has remained concentrated in the range of mean anomaly owing to its young age. In particular, it is interesting that Spurný et al. (2017) noted that the 1995 detected Taurid fireballs did not quite have the orbital elements of the 2015 Taurids. They had larger semimajor axes

Table 4
Poisson Test on the Significance of the Impact Rate Increase of Meter-sized Weak Material (Peak Brightness >60 km) Hitting Earth Observed by the USGS during STS Outburst Episodes ($\lambda_\odot \in [213, 234]^\circ$)

Population	Surveyed Years	Observed Events	$\lambda_\odot$ Integrated (deg)	Rate (Earth$^{-1}\lambda_\odot^{-1}$)
Weak impactor population	[2005–2016]	10	3960	[0.001–0.005]
Probable STS	2005, 2008, 2012, 2015	3	84	[0.007–0.1]

Note. Ranges given are at 2σ confidence. The influx increase factor during an STS outburst is [2.1, 46]×.

and smaller perihelia that did not change so much with solar longitude. This could point to the presence of streams being more dispersed but narrow, which occasionally wander in Earth's path.

4.2. Meteorite Dropping Taurids?

Brown et al. (2013) identified the Taurid showers as a potential source of macroscopic meteorite dropping events if a large enough meteoroid enters Earth's atmosphere. We have seen that the STS branch contains large members; do members of that population have a chance of surviving entry and falling as a meteorite? Large s-Taurids behave like weak matter (Figure 5). They experience catastrophic disruption at very high altitudes (>66 km; see Table A1). Their weak nature is not compensated by size, as Spurný et al. (2017) noted that the larger s-Taurids tend to be the weaker ones. The deepest penetrating STS observed by the DFN (*DN*151114_04) is not visible below 52 km. According to the criteria of Brown et al. (2013), which states that a height of 35 km and velocity of 10 km s^{-1} are approximate terminal dynamical criteria for a given event to have a chance of producing a meteorite fall, this is unlikely to produce a recoverable meteorite on the ground. The two very bright STSs described by Olech (2016) and Spurný et al. (2017) also terminate at high altitudes of 57.86 and 60.20 km.

Is this weakness a feature of all Southern Taurids? The deepest penetrating Southern Taurid (MORP #715) described in the MORP data set (Halliday et al. 1996) only penetrates to 54.8 km. As outlined by Brown et al. (2013), one of the EN fireballs in 1995 penetrated as deep as 30 km. Although this fireball was tentatively linked to the Taurid Complex, no definite association with either branch of the Taurids was reported, and the final velocity was not reported either. More generally, to our knowledge there is no report in the literature of a Southern Taurid that comes close to the terminal parameter of Brown et al. (2013).

On the other hand, we have examples of Northern Taurids that are able to penetrate much lower than the 50 km ceiling that Southern Taurids seem to hit. For example, on 2016 October 9, the DFN observed a Northern Taurid penetrating as deep as 36.4 km, slowing down to 9.7 km s^{-1}; the terminal parameters for this NTA are much closer to the cutoff criteria of Brown et al. (2013), but still greater than required for a meteorite to survive. Are we seeing inhomogeneities here in the original composition of 2P/Encke? Or are the stronger materials representative of older meteoroids that survived the harsh conditions in the interplanetary medium?

5. Conclusions

The periodic outbursts of Taurid fireballs and visible meteors are from a stream called the s-Taurids (IAU shower 628, STS). The shower stands out well as a concentration of orbits in speed versus solar longitude diagram, with the shower members having a strongly changing entry speed with position along Earth's orbit.

We have established the size–frequency distribution for the s-Taurid stream. Even at gram sizes, the stream shows a very shallow distribution with a magnitude distribution index of 2.0 (differential mass distribution index of $s = 1.75$), atypical of other JFC showers. The distribution appears to remain unchanged up to meter-sized fragments.

The highly stratified structure of this stream, as well as the shallow size–frequency distribution remaining constant over a large range in size, points to the stream being the product of a gentle and relatively recent breakup.

Because the meteoroids initially move on different orbits than 2P/Encke, the breakup involved a different parent body. That body consisted of weak material. The distribution of longitude of perihelion along Earth's orbit points to the stream having originated from surviving asteroid *2015 TX24*, a low albedo 0.07, 0.25 ± 0.04 km sized ($H = 21.5$) asteroid that is a good candidate for a 2P/Encke sibling, together with *2014 TG10* and other such bodies identified earlier. 2015 TX24, 2005 UR, and 2005 TF50 may have broken from a common body 1500 yr ago, with recent activity from 2015 TX24 now producing the meteoroids detected at Earth as the s-Taurids.

.Large meter-sized bodies survive in the s-Taurids, possibly because they represent relatively strong cometary materials. During the s-Taurid #628 stream (STS) outburst years, the chance of Earth being hit by a meter-scale weak meteoroid is enhanced by a factor of at least [2.5, 55]. Earth encounters the STS stream on average every 5 yr; therefore, the STS stream is responsible for as much as 20% of all weak (airburst >60 km altitude) meter-scale bodies.

From the analysis of terminal parameters (heights and speeds) of the large Taurid meteoroids observed by the DFN, a macroscopic meteorite from a Southern Taurid stream seems unlikely; on the other hand, we have examples of Northern Taurids that approach the meteorite dropping terminal parameters discussed by Brown et al. (2013). Given their shallow penetration depth, large meteoroids from the s-Taurids are unlikely to drop meteorites but might generate dust that can be collected in the atmosphere.

When the cloud of meteoroids next returns close to Earth in 2022, the Large Synoptic Survey Telescope (Ivezic et al. 2008) will be up and running and should be able to better constrain the hypothetical population of meter-sized s-Taurids. The recently commissioned Geostationary Lightning Mapper (Jenniskens et al. 2018) should also be able to fill the observation gap around the decimeter scale and notably provide a good estimate of the flux density of STS meteoroids in this range.

This research is supported by the Australian Research Council through the Australian Laureate Fellowship's scheme, receives institutional support from Curtin University, and uses the computing facilities of the Pawsey supercomputing center. The DFN data reduction pipeline makes intensive use of Astropy, a community-developed core Python package for Astronomy (Astropy Collaboration et al. 2013). P.J. is supported by grant 80NSSC19K0513 of NASA's Emerging Worlds program and grant 80NSSC19K0563 of NASA's Solar System Workings program.

Appendix

The key parameters for the fireballs observed by the DFN are available in machine-readable form online; Table A1 is the corresponding metadata/documentation.

Table A1
Desert Fireball Network Fireball Catalog

Column	Label	Units	Description
1	Dur	s	Observed duration of the meteor
2	SLONG	deg	Solar longitude
3	IniH	m	First observed height
4	IniLon	deg	First observed longitude
5	IniLat	deg	First observed latitude
6	IniVel	m s^{-1}	Observed initial speed
7	e_IniVel	m s^{-1}	1σ uncertainty on observed initial speed
8	EndH	m	Last observed height
9	Endlon	deg	Last observed longitude
10	EndLat	deg	Last observed latitude
11	Slope	deg	Trajectory inclination wrt to horizon
12	BCAngle	deg	Best trajectory convergence angle between observation planes
13	IntBright	m	Closest observation range at the first observed point
14	EndBright	m	Closest observation range at the final observed point
15	MajAxis	au	Semimajor axis of the heliocentric orbit
16	e_MajAxix	au	
17	ecc		Eccentricity of the orbit
18	e_ecc		d
19	inc	deg	Inclination of the orbit (J2000)
20	e_inc	deg	
21	ArgPeri	deg	Argument of periapsis (J2000)
22	e_ArgPeri	deg	
23	longAsc	deg	Longitude of the ascending node (J2000)
24	e_longAsc	deg	
25	RAdeg	deg	Right ascension of the radiant at 1 au
26	e_RAdeg	deg	
27	DEdeg	deg	Declination of the radiant at 1 au
28	e_DECedg	deg	
29	Vel	m s^{-1}	Speed at 1 au
30	e_Vel	m s^{-1}	
31	Tj		Tisserand parameter wrt Jupiter
32	HPeak	m	Altitude of the point of peak brightness
33	Vmag	mag	Maximum absolute magnitude (normalized to 100 km distance)

(This table is available in its entirety in machine-readable form.)

ORCID iDs

Hadrien A. R. Devillepoix https://orcid.org/0000-0001-9226-1870
Eleanor K. Sansom https://orcid.org/0000-0003-2702-673X
Martin C. Towner https://orcid.org/0000-0002-8240-4150
Patrick Shober https://orcid.org/0000-0003-4766-2098
Trent Jansen-Sturgeon https://orcid.org/0000-0002-0363-0927

References

Asher, D. J., Clube, S. V. M., & Steel, D. I. 1993, MNRAS, 264, 93
Asher, D. J., & Izumi, K. 1998, MNRAS, 297, 23
Astropy Collaboration, Robitaille, T. P., Tollerud, E., et al. 2013, A&A, 558, A33
Babadzhanov, P. B., & Kokhirova, G. I. 2009, A&A, 495, 353
Beech, M., Hargrove, M., & Brown, P. 2004, Obs, 124, 277
Blaauw, R. C., Campbell-Brown, M., & Kingery, A. 2016, MNRAS, 463, 441
Borovička, J. 1990, BAICz, 41, 391
Borovička, J., & Spurný, P. 2020, P&SS, 182, 104849
Bronshten, V. A. 1981, AVest, 14, 44
Brown, P., Marchenko, V., Moser, D. E., Weryk, R., & Cooke, W. 2013, M&PS, 48, 270
Brown, P., Spalding, R. E., ReVelle, D. O., Tagliaferri, E., & Worden, S. P. 2002, Natur, 420, 294
Brown, P., Wiegert, P., Clark, D., & Tagliaferri, E. 2016, Icar, 266, 96
Ceplecha, Z., & McCrosky, R. E. 1976, JGR, 81, 6257
Clube, S. V. M., & Napier, W. M. 1984, MNRAS, 211, 953
Devillepoix, H. A. R., Bland, P. A., Sansom, E. K., et al. 2019, MNRAS, 483, 5166
Devillepoix, H. A. R., Sansom, E. K., Bland, P. A., et al. 2018, M&PS, 53, 2212
Drummond, J. D. 1981, Icar, 45, 545
Dubietis, A., & Arlt, R. 2007, MNRAS, 376, 890
Fay, M. P. 2010, The R Journal, 2, 53
Froeschle, C., & Scholl, H. 1986, A&A, 158, 259
Grün, E., Zook, H. A., Fechtig, H., & Giese, R. H. 1985, Icar, 62, 244
Halliday, I., Griffin, A. A., & Blackwell, A. T. 1996, M&PS, 31, 185
Hasegawa, I. 1990, PASJ, 42, 175
Howie, R. M., Paxman, J., Bland, P. A., et al. 2017a, ExA, 3, 237
Howie, R. M., Paxman, J., Bland, P. A., et al. 2017b, M&PS, 52, 1669
Ivezic, Z., Axelrod, T., Brandt, W. N., et al. 2008, SerAJ, 176, 1
Jansen-Sturgeon, T., Sansom, E. K., & Bland, P. A. 2019, M&PS, 54, 2149
Jenniskens, P. 2006, Meteor Showers and Their Parent Comets (Cambridge: Cambridge Univ. Press)
Jenniskens, P., Albers, J., Tillier, C. E., et al. 2018, M&PS, 53, 2445
Jenniskens, P., Gural, P. S., Dynneson, L., et al. 2011, Icar, 216, 40
Jenniskens, P., Nénon, Q., Albers, J., et al. 2016a, Icar, 266, 331
Jenniskens, P., Nénon, Q., Gural, P. S., et al. 2016b, Icar, 266, 355
Jenniskens, P., Nénon, Q., Gural, P. S., et al. 2016c, Icar, 266, 384
Jenniskens, P., Utas, J., Yin, Q.-Z., et al. 2019, M&PS, 54, 699
Madiedo, J. M., Ortiz, J. L., Trigo-Rodríguez, J. M., et al. 2014, Icar, 231, 356
Moorhead, A. V., Egal, A., Brown, P. G., Moser, D. E., & Cooke, W. J. 2019, JSpRo, 56, 1531
Neslusan, L., Svoren, J., & Porubcan, V. 1998, A&A, 331, 411
Nesvorný, D., & Morbidelli, A. 1998, AJ, 116, 3029
Olech, A., Żołądek, P., Wiśniewski, M., et al. 2016, MNRAS, 461, 674
Olech, A., Żołądek, P., Wiśniewski, M., et al. 2017, MNRAS, 469, 2077
Picone, J. M., Hedin, A. E., Drob, D. P., & Aikin, A. C. 2002, JGRA, 107, 1468
Popescu, M., Birlan, M., Nedelcu, D. A., Vaubaillon, J., & Cristescu, C. P. 2014, A&A, 572, A106
Sansom, E. K., Bland, P., Paxman, J., & Towner, M. 2015, M&PS, 50, 1423
Sansom, E. K., Bland, P. A., Towner, M. C., et al. 2020, M&PS, 55, 2157
Shrbený, L., & Spurný, P. 2012, LPICo, 1667, 6436
Soja, R. H., Baggaley, W. J., Brown, P., & Hamilton, D. P. 2011, MNRAS, 414, 1059
SonotaCo. 2009, JIMO, 37, 55
Southworth, R. B., & Hawkins, G. S. 1963, SCoA, 7, 261
Spurný, P. 1997, P&SS, 45, 541
Spurný, P., Borovička, J., Mucke, H., & Svoreň, J. 2017, A&A, 605, A68
Tagliaferri, E. 1994, in Hazards Due to Comets and Asteroids, ed. T. Gehrels, M. S. Matthews, & A. Schumann (Tucson, AZ: Univ. Arizona Press)
Towner, M., Cupak, M., Deshayes, J., et al. 2020, PASA, 37, e008
Tubiana, C., Snodgrass, C., Michelsen, R., et al. 2015, A&A, 584, A97
Whipple, F. 1940, Proc. of the American Philosophical Society, 83, 711, http://www.jstor.org/stable/985135
Whipple, F. L., & El-Din Hamid, S. 1952, HelOB, 41, 3